CHAPTER 1

INTRODUCTION AND LITERATURE REVIEW

1.1 Development of Aluminium and Aluminium Alloys

Aluminium alloys have been one of the most popular material for structural components in engineering industry like aerospace, automotive and construction from the last few decades. The most characteristic properties of aluminium is its low density and in addition, aluminium has excellent corrosion resistance, high specific strength and specific stiffness, good formability, high electrical and thermal conductivity. Aluminium alloys can be heat treated to high-strength levels and easily fabricated. Low modulus of elasticity, low elevated temperature properties and high susceptibility of high strength aluminium alloys to stress corrosion are their disadvantages [1].

The modern philosophy of the aerospace industry is high pay load and reduced cost of transportation. One way to achieve this is to reduce the weight of the aircraft. Aluminium alloys have been the main airframe material after the replacement of wood by them in 1920. Dramatic improvements have occurred in aluminium alloys since they were first introduced in the 1920s. Fig. 1.1 shows the improvement in aluminium alloys as a result of continued research related to chemical composition, control of impurities and the effect of heat treatment and processing. The chemical compositions of some aerospace grade aluminium alloys are given in Table 1.1 [2].

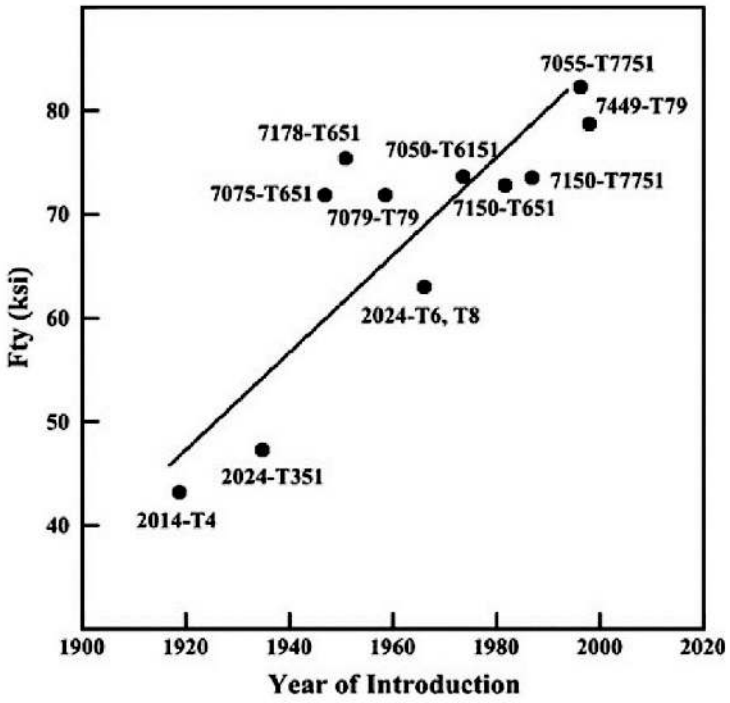

FIGURE 1.1: Yield strength versus year of introduction of aluminium alloy [2]

Many investigations found that aluminium alloys containing both zinc and magnesium developed substantially higher strength than those containing either of the alloying elements added singly. These findings led to development of the Al–Zn–Mg–Cu alloy AA7075 in the early 1940s followed by the development of higher strength alloy AA7178 [3]. However, low toughness led to development of alloys with much lower Fe and Si contents, e.g. AA7050 and AA7475. 7xxx series alloys are often used for high strength applications, predominantly in compressively loaded airframe structures, such as, upper wing panels, frames, stringers, longerons, extruded parts, etc.

TABLE 1.1: Chemical composition of some important aluminium alloys [2].

Alloy	Cu	Mg	Zn	Mn	Si	Fe	Cr	Ti	Zr
AA2014	3.9-5.0	0.2-0.8	0.25_{max}	0.4-1.2	0.5-1.2	0.7_{max}	0.10_{max}	0.15_{max}	-
AA2017	3.5-4.5	0.4-0.8	0.25_{max}	0.4-1.0	0.2-0.8	0.7_{max}	0.10_{max}	0.15_{max}	-
AA2024	3.8-4.9	1.2-1.8	0.25_{max}	0.3-0.9	0.50	0.50	0.10	0.15	-
AA2219	5.8-6.8	0.02_{max}	0.10_{max}	0.2-0.4	0.20_{max}	0.30_{max}	-	0.02-0.10	0.1-0.25
AA5083	0.10_{max}	4.0-4.9	0.25_{max}	0.4-1.0	0.40_{max}	0.40_{max}	0.05-0.25	0.15_{max}	-
AA6061	0.15-0.4	0.8-1.2	0.25_{max}	0.15_{max}	0.4-0.8	0.7_{max}	0.04-0.35	0.15_{max}	-
AA7050	2.0-2.6	1.9-2.6	5.7-6.7	0.1_{max}	0.12_{max}	0.15_{max}	0.04_{max}	0.10_{max}	0.08-0.15
AA7075	1.2-2.0	2.1-2.9	5.1-6.1	0.3_{max}	0.4_{max}	0.5_{max}	-	0.10_{max}	-
AA7150	1.9-2.5	2.0-2.7	5.9-6.9	0.10	0.12	0.15	0.04	0.08-0.15	0.06
AA7178	1.6-2.4	2.4-3.1	6.3-7.3	0.30	0.4	0.5	0.18-0.28	0.20	-
AA7475	1.2-1.9	1.9-2.6	5.2-6.2	0.06_{max}	0.1_{max}	0.12_{max}	0.18-0.25	0.06_{max}	-

The new generation of aircrafts, like A380, still contain 60% of the traditional aluminium alloys [4]. Though the role of aluminium in future aircraft will probably be somewhat diminished due to increasing use of composite materials, the high-strength aluminium alloys are, and will remain, important airframe materials.

As the aircraft became larger in size it became necessary to use thicker-section airframe components. However, thick-section products of the high-strength 7XXX alloys like AA7075-T6 and particularly AA7079-T6 were found to be susceptible to stress corrosion cracking (SCC) in the short transverse direction. The overaged T73 and T76 tempers were developed in the early 1960s to make AA7075 more resistant to SCC and exfoliation corrosion.

Subsequently the alloy AA7475 was developed from AA7075 with improved fracture toughness. Then a new generation of alloys, including AA7050-T7351, was developed during the 1970s to fit the need for a material that would develop high strength in thick-section products, good resistance to SCC and exfoliation corrosion, as well as good fracture toughness and fatigue characteristics. These developments are continuing and one of the latest alloys is AA7085.

1.2 Typical Aerospace Applications of Aluminium Alloys

Even in the fighter aircraft, which already have composite material percentages in the range of 40-50%, aluminium alloys still play a significant role [5]. The attractiveness of aluminium alloys is that they are low cost, lightweight and can be heat treated to fairly

FIGURE 1.2: Engineering properties required for main structural components [4].

high-strength levels. Also they are one of the most easily fabricated high performance materials with relatively low cost of manufacturing. More specifically, the requirements of alloy property vary depending on the application. A generic example is shown in Fig. 1.2, which elucidates the engineering property requirements for several of the main structural areas in a transport aircraft, namely (i) fuselage and pressure cabins, (ii) wings and (iii) empennage (horizontal and vertical stabilizers). The engineering properties required for these structures are tensile strength (TS), cyclic yield strength (CYS), stiffness, damage tolerance against fatigue, fatigue crack growth and fracture toughness, and also the resistance against general and stress corrosion cracking. The rankings of the requirements differ for different areas, but there is much commonality.

TABLE 1.2: Conventional aluminium alloys in airframe components with their application [6]

Product	Strength levels	Alloy/temper	Applications
Sheet	Damage tolerant	2024-T3, 2524-T3/351	Fuselage/ pressure cabin skin
Plate	Damage tolerant	2024-T351, 2324-T39, 2624-T351, 2624-T39	Lower wing covers
	Medium strength	2024-T62	Tactical aircraft fuselage panels
	Medium strength	2124-T851	Tactical aircraft bulkheads
	Medium strength	7050-T7451, 7X75-T7XXX	Internal fuselage structures
	High strength	7150-T7751, 7055-T7751, 7055-T7951, 7255-T7951	Upper wing covers
	Medium strength	7050-T7451	Spars, ribs, other internal structures
Forgings	High strength	7175-T7351, 7050-T7452	Wing/ fuselage attachments
Extrusions	Damage tolerant	2024-T3511, 2026-T3511, 2024-T4312, 6110-T6511	Lower wing stringers Fuselage/pressure cabin stringers
	Medium/high strength	7075-T73511, 7075-T79511, 7150-T6511, 7175-T79511, 7055-T77511, 7055-T79511	Fuselage stringers and frames, upper wing stringers, floor beams,seat rails

Table 1.2 presents a survey of the actual and proposed uses of the conventional 2XXX and 7XXX aluminium alloys in airframe structures. Alloy producers develop basically similar alloys for different product forms and applications. The most important contribution to this flexibility is the development of a range of alloy tempers that allow optimizations and trade-offs of properties, and hence the ability to match the alloys to particular applications.

1.3 Classification of Aluminium Alloys

Aluminium alloys are categorized either as heat treatable or non-heat treatable, depending whether or not they respond to precipitation hardening [5,7]. The heat treatable alloys contain elements that decrease in solid solubility with decreasing temperature, and in concentrations that exceed their equilibrium solid solubility at room temperature and moderately higher temperatures. The most important alloying elements are copper, lithium, magnesium and zinc. Some cast alloys are essentially non-heat-treatable and are used as-cast or in thermally modified conditions uninfluenced by solutionizing or precipitation effects [2]. A large number of other compositions rely instead on work hardening through mechanical reduction, usually in combination with various annealing procedures for property developments. These alloys are referred to as non-heat-treatable or work-hardening alloys. Fig. 1.3 gives an overview of the principal types of aluminium alloys.

Most alloys with aluminium and relatively few have sufficient solid solubility to assist as major alloying additions (Table 1.3). Transition metals like chromium, manganese

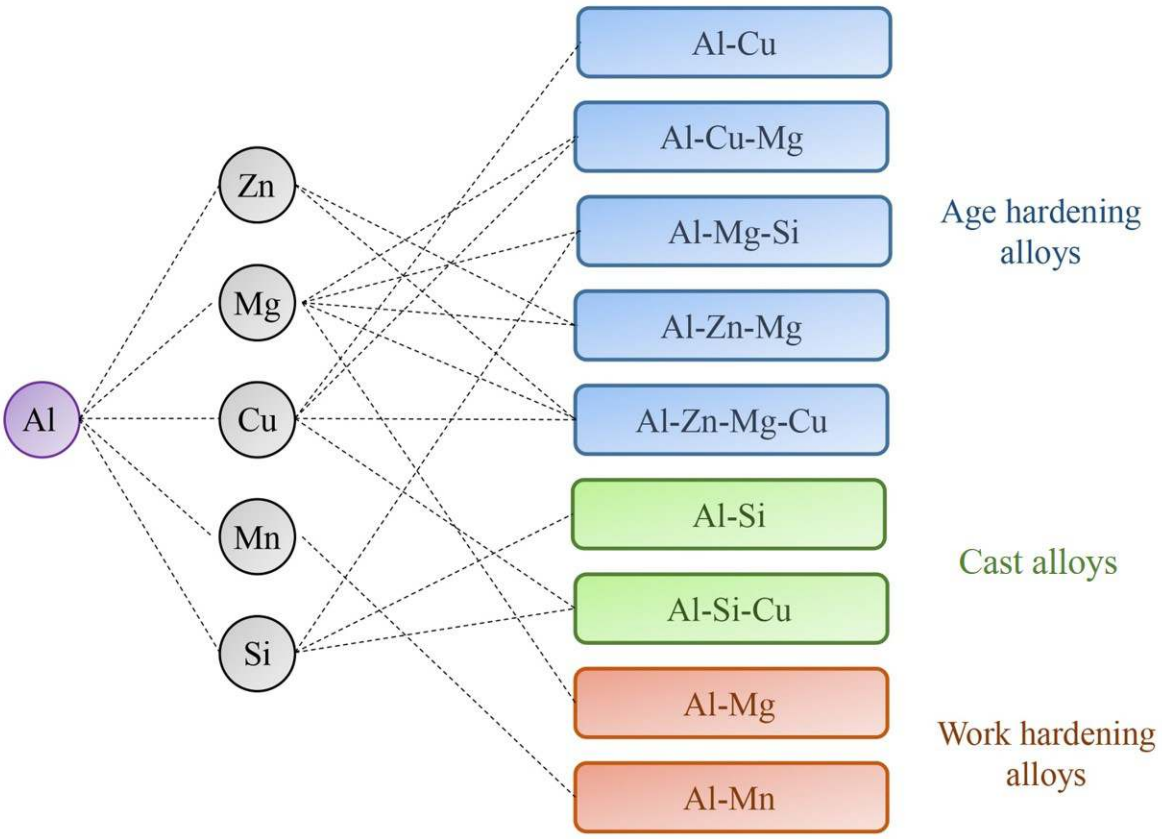

FIGURE 1.3: Primary types of aluminium alloys [8].

and zirconium, having solid solubility below 1 at.% confer important improvements to alloy properties by forming intermetallic compounds that control the microstructure. Apart from tin, which is sparingly soluble, the maximum solid solubility in binary aluminium alloys occurs at the eutectic and peritectic temperatures [8]. The heat treatment given to aluminium alloys to increase strength is age hardening. The basic requirement for an alloy to be responsive to age-hardening is a decrease in solid solubility of one or more of the alloying elements with decreasing temperature.

TABLE 1.3: Solid solubility of different elements in aluminium [8]

Element	Temperature for maximum solid solubility (°C)	Maximum solid solubility	
		(wt.%)	(at.%)
Cadmium	649	0.4	0.09
Cobalt	657	<0.02	<0.01
Copper	548	5.65	2.40
Chromium	661	0.77	0.40
Germanium	424	7.2	2.7
Iron	655	0.05	0.025
Lithium	600	4.2	16.3
Magnesium	450	17.4	18.5
Mangnese	658	1.82	0.90
Nickel	640	0.04	0.02
Silicon	577	1.65	1.59
Silver	566	55.6	23.8
Tin	228	$\sim$ 0.06	$\sim$ 0.01
Titanium	665	$\sim$ 1.3	$\sim$ 0.74
Vanadium	661	$\sim$ 0.4	$\sim$ 0.21
Zinc	443	82.8	66.4
Zirconium	660.5	0.28	0.08

1.4 Physical Metallurgy of Al-Zn-Mg-Cu Alloys

The Al–Zn–Mg system offers greatest potential among all aluminium alloys for age-hardening even though the very high-strength alloys always contain quaternary additions of copper for the improvement in stress-corrosion cracking. The formation of supersaturated solid solution during quenching from high temperature is due to the presence of a good solid solution range in 7xxx series alloys [8]. These alloys are also unstable after quenching and natural aging occurs even at room temperature. During aging, precipitation reaction results in the formation of precipitate phases. The mechanism of homogenous precipitation in 7xxx series alloys can be shown as:

Supersaturated Solid Solution (SSS) $\rightarrow$ Guinier-Preston (GP) zones $\rightarrow$ non-equilibrium

(metastable) phase (η') $\rightarrow$ equilibrium precipitate (η). The increase in vacancy concentration of supersaturated solid solution increases the homogenous precipitation by forming the clusters of vacancies and solute diffusion to vacancy clusters for the formation of GP zones. The diffusion of solutes causes the growth of GP zones to intermediate precipitates with the continuous aging process. These metastable (η') phases are spherical in shape. An increase in internal stress occurring due to the intermediate precipitates results in the partial loss of coherency with the matrix phase. The equilibrium precipitate η or T/E phase (which are coherent with the matrix) forms with the continuous aging process.

The composition of the intermediate precipitate η' cannot be stated clearly as previous studies report the composition of η' similar to the equilibrium precipitate. A few other researchers have reported the composition of η' having Zn:Mg ratio 1:1 which is closer to GP zone [9–11]. Equilibrium precipitate is hexagonal in shape with composition $MgZn_2$, where Zn:Mg ratio is 2:1. The optimum strength of 7075 and 7050 alloys is obtained from intermediate precipitates and GP zones. However, the precipitates grow to equilibrium precipitates due to continuous aging which causes the loss in strength.

Grain boundary precipitate structures are also modified by precipitation hardening. Although 7075 and 7050 alloys are vulnerable to intergranular corrosion like SCC, therefore, heat treatments are considered to develop the precipitate structure for preventing the continuous corrosion path at grain boundaries. In the 1960's, the stress corrosion cracking to the requirement of 7075-T6 thicker sections in aircraft designs, resulted in the development of 7075-T73 temper. 7075-T73 forgings were developed using a two step aging heat treatment process for improvement of the corrosion resistance. After aging at around

120°C for 24 h, the T7 temper was obtained by over aging above 150°C for 7-9 h for improving the stress corrosion cracking resistance [12].

There is an inverse relationship between strength and SCC resistance in T6 and T73 tempers, which can be seen in Fig. 1.4 [12]. From the Fig. 1.4, it can be observed that strength decreases whereas the resistance to SCC increases with increasing the aging temperature and time. In this figure, the initial aging gap is shown by stage I and stage II can be related to T6 temper. Stage II shows that the higher strength can be obtained but the resistance to SCC is low. In stage III, it is shown that the prolonged aging can increase SCC resistance but there is also a loss of strength.

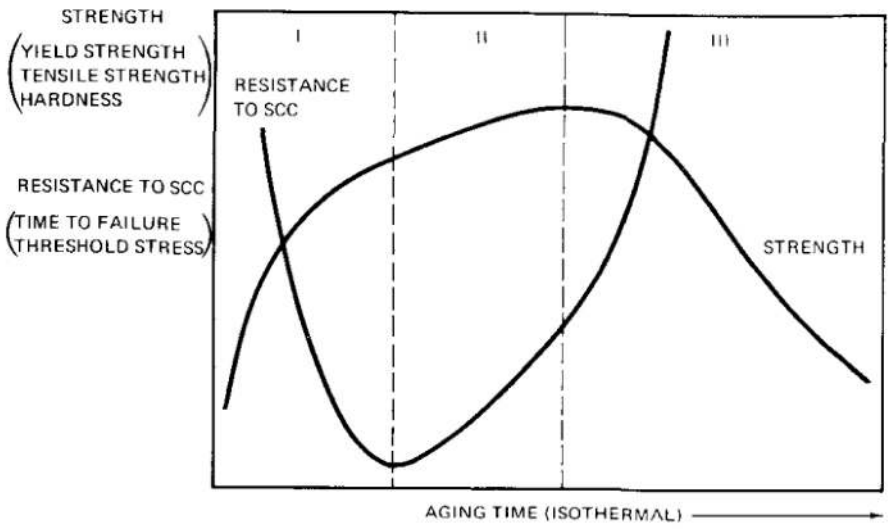

FIGURE 1.4: Variation of resistance to SCC and strength with aging time [12].

In the 1970's, heat treatment 'Retrogression and Reaging (RRA)' was developed by Cina [12] to deal with the trade-off between strength and stress corrosion resistance in the tempers T6 and T73. This heat treatment is applied to 7075-T6 which includes 'retrogression' (known as partial re-solutionizing) of the T6 temper which occurs at a

higher temperature for a very short time duration (example 200°C/2 minutes, 240°C/7 sec.). During retrogression, the dissolution of strengthening precipitate phase and dislocations occur which results in a loss of strength (Fig. 1.4) [12]. This process is followed by reaging using the aging conditions of temper T6 (121°C for 24 hours) to achieve a better combination of strength and SCC resistance [13, 14]. From Fig. 1.5, the effect of retrogression time on hardness after retrogression and subsequent reaging can be seen. It was observed that after a short retrogression time, strength reaches the lowest minimum whereas the increase in retrogression time results in an increase in hardness. A further increase in retrogression time causes decrease in the hardness. Subsequent reaging increases the hardness. However, at the lowest minimum on retrogression curve corresponding to few seconds of retrogression results in higher strength after reaging.

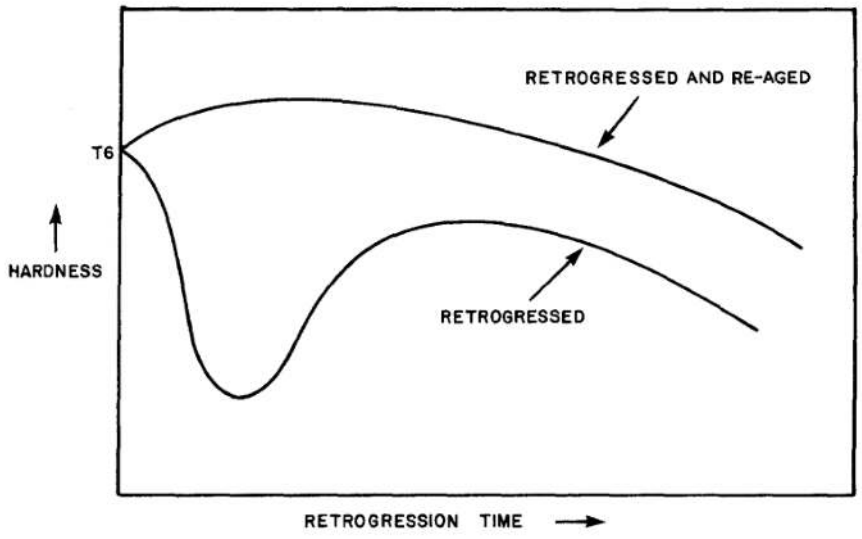

FIGURE 1.5: Variation of hardness during RRA heat treatment [12].

1.4.1 Mechanism of precipitation hardening in 7xxx alloys

In 7xxx alloys, the interaction between dislocation and second phase particles formed during precipitation causes increase in strength. Parameters like spacing, size, and degree of coherency between the precipitate and the matrix determine the dislocation-precipitate interaction. Depending on the alloy, strength is determined by the ability to resist dislocation motion through the following mechanisms [15, 16]:

Strain fields formed by coherent GP zones: Strain fields are generated due to the presence of a misfit between the matrix and the precipitate which increases the internal stress. Higher stress will be needed for the dislocation motion, thus strength will increase.

Shearing of deformable precipitates: Interaction between small precipitates and dislocations is often by shearing. This happens due to the deformability of small precipitates which allows dislocations to pass through the precipitates. The stress required to initiate dislocation motion is called critically resolved shear stress (CRSS). CRSS is low in the initial stage of precipitate growth and this enables the dislocations to shear through precipitates. This type of interaction is also recognized as chemical hardening. During this interaction, formation of an additional interface causes changes along the slip plane. Strength is also increased and more work will be required to achieve the changes.

Bypass of coarse, non-deformable precipitates: Dislocations find a way around coarse particles due to the increase in particle spacing and loss of coherency at the interface of matrix and precipitate. Resistance to shearing from dislocations increases with the growth of precipitates. Strengthening is achieved due to the work hardening by dislocation of debris left after particles looping by dislocation. From Fig. 1.6, it is seen that

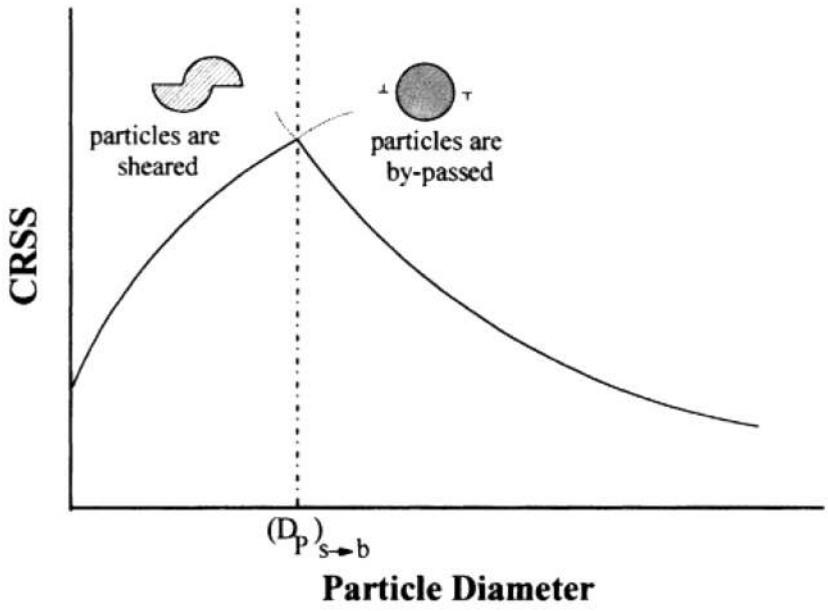

FIGURE 1.6: Effect of particle diameter and CRSS on dislocation-precipitate interaction [1].

the particle size affects the CRSS in deformable and non-deformable particles with the growth of precipitate particles [9]. As shown in this figure, the critical particle size correlates to the high critical resolved shear stress. High strength can be obtained at the critical particle size due to the difficulty in attaining the high CRSS.

1.4.2 Microstructural features

The properties of 7xxx series alloys are affected by some microstructural features. Among all, some important features like dispersoids, intermetallic compounds, constituent particles, grain boundary and matrix precipitates among others are also important which affect the properties such as strength, fracture toughness and corrosion resistance of the 7xxx alloys.

Matrix and grain boundary precipitate: The properties of 7xxx alloys can be affected by the composition, structure and distribution of precipitates in the matrix and grain boundary region. Among other factors of a microstructure, matrix precipitates affect the

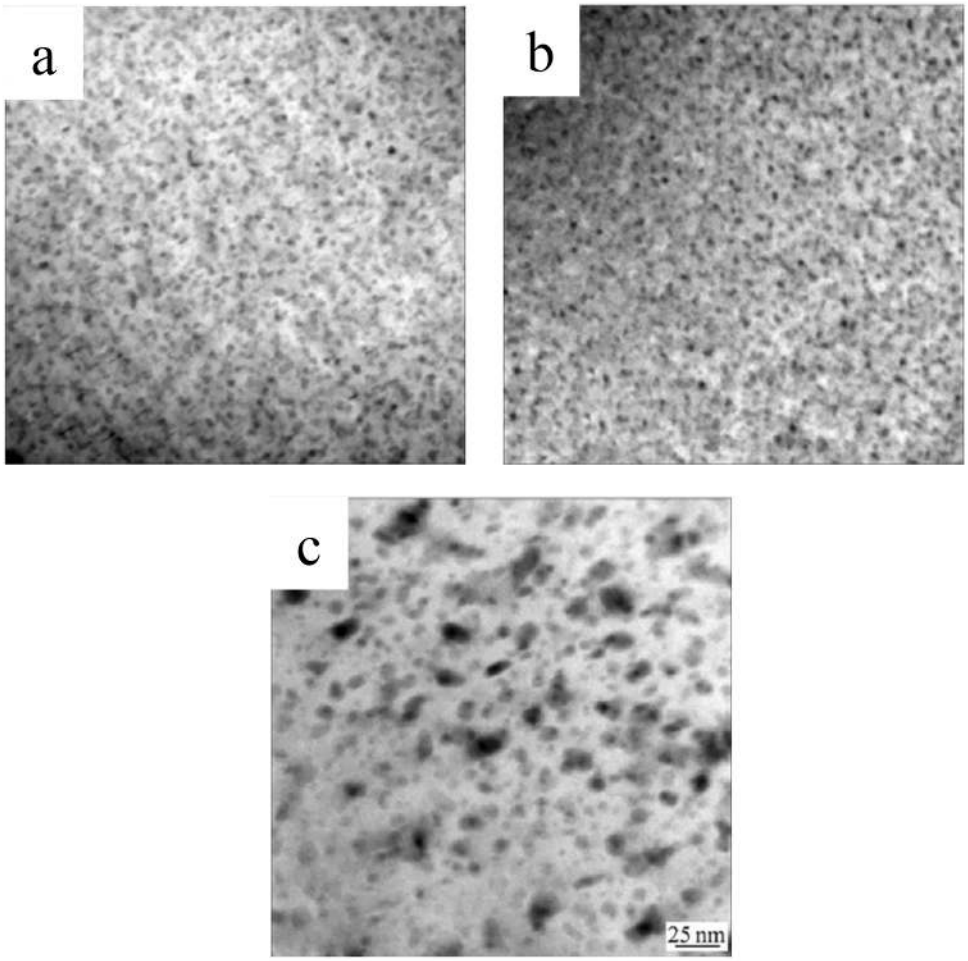

FIGURE 1.7: Distribution of precipitates within the matrix in (a) T6, (b) RRA and (c) T7 temper respectively [17].

strength whereas the grain boundary precipitates affect the resistance to intergranular corrosion [17, 18]. Coherent precipitates are finely distributed in the matrix to restrict the dislocation motion for achieving high strength during aging. The loss in strength and

coherency arises due to the increase in precipitate size in matrix and grain boundary region, emerged by continuous aging to the overaged condition. The morphology of fine and coarse precipitates is shown in Fig. 1.7 for T6, RRA and T7 condition, respectively. The high concentration of fine precipitates in T6 and RRA causes increase in the strength whereas precipitate coarsening in the T7 temper causes the loss of strength [17]. Fig. 1.8

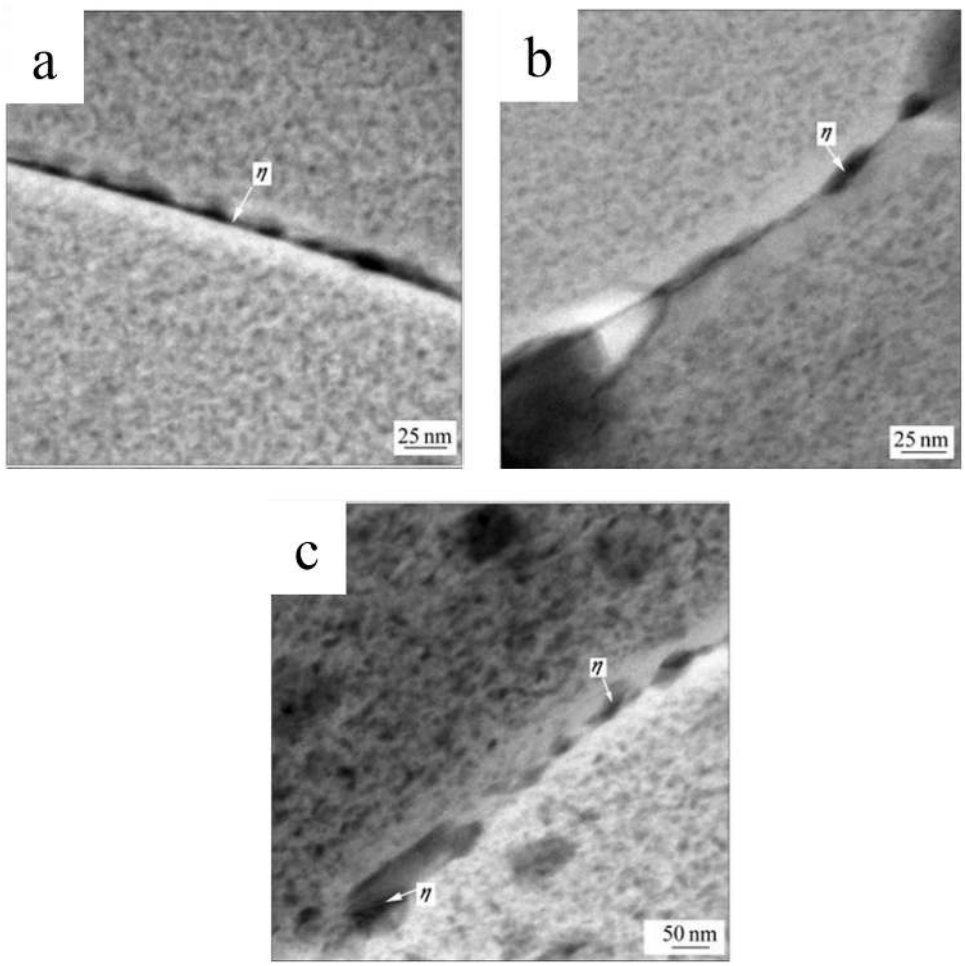

FIGURE 1.8: Distribution of grain boundary precipitates in (a) T6, (b) RRA and (c) T7 temper respectively [17].

shows the morphology of grain boundary precipitates in temper T6, RRA and T7, respectively. In T6, continuous distribution of small precipitates is observed whereas in RRA

and T7, a discontinuous distribution of coarse precipitates is observed. The resistance to intergranular corrosion is improved due to coarsening of precipitates in the grain boundary during overaging by eliminating a continuous path for corrosion to occur [18]. Studies based on other heat treatment procedure adopted for improving the SCC resistance like retrogression and reaging show the discontinuous distribution of coarse precipitates along the grain boundary [17].

Constituent particles: Constituent particles are intermetallic compounds which are formed during solidification through eutectic reactions. These particles may have Si or Fe with other alloying elements and aluminium at times. Constituent particles with Fe are insoluble whereas those without Fe may be completly or slightly soluble, based on solute content in the solid solution [9]. Larger constituent particles (diameter >1 μm) are undesirable in aluminium alloys. Constituent particles are not effective strengthening particles due to the incoherency with matrix phase. These particles can support crack growth and reduce fatigue resistance and fracture toughness. In 7075 alloy, SiO_2, Al_7Cu_2Fe, $Al_{12}(Fe, Mn)_3Si$, $Al_6(Fe, Mn)$, $Al_{23}CuFe_4$ and Mg_2Si, are the common known constituent particles [9]. The compositional modification by lower amounts of Fe and Si in 7050 alloy attains the decrease in the constituent particle numbers and size in 7050 alloy. Al_7Cu_2Fe, Al_2CuMg and Mg_2Si are commonly formed in 7050 alloy [9].

Dispersoids: Dispersoids are those small particles which are formed by aluminium and transition metal alloying elements such as Cr, Mn and Zr during hot rolling. These particles are helpful in preventing the recrystallization by pinning the grains movement due to their small size and fine distribution. The ability of dispersoids in preventing the

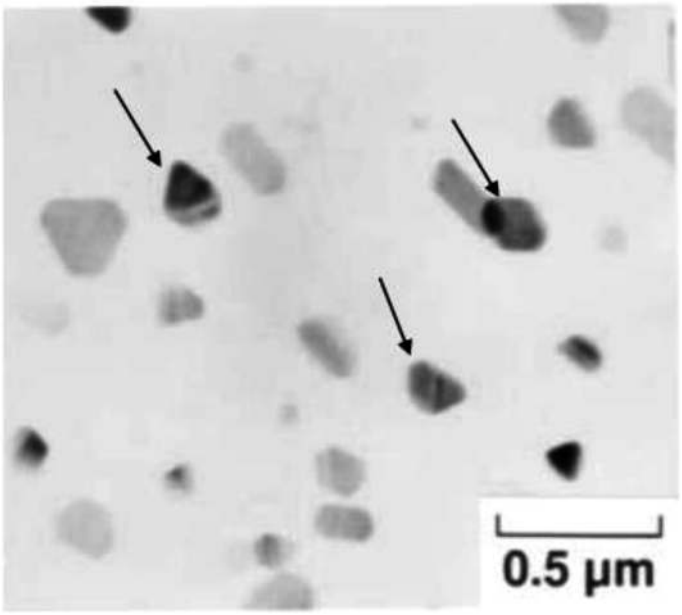

FIGURE 1.9: Dispersoid of $Al_{12}Mg_2Cr$ in alloy 7075 [9].

recrystallization needs small size, small spacing and coherent or semi-coherent interface with the matrix. However, dispersoids can nucleate microvoids which is undesirable. In 7075 alloy, a common dispersoid $Al_{12}Mg_2Cr$ can be seen in Fig. 1.9 [9]. Al_3Zr is a common precipitate in 7050 alloy and other aluminium alloys of high strength. The quench sensitivity of an alloy can be affected by the type of dispersoids formed.

1.5 The Process of Grain Refinement at Surface

Nanostructured materials are defined as solids with grain, subgrain, twin, or dislocation cells with sizes below 100 nm. Such materials usually have superior mechanical and physical properties, including high strength, improved corrosion resistance, and higher wear resistance. Two complementary approaches have been developed for synthesizing nanostructured solids. The first is the "bottom-up" approach, in which nanostructured

materials are assembled from individual atoms or from nanoscale building blocks such as nanoparticles. The second is the "top-down" approach, in which existing coarse grained materials are processed to produce substantial grain refinement and nanostructure. The most successful top-down approaches involve the application of large plastic deformation, in which materials are subjected to plastic strains.

Various surface modification techniques have been developed to produce nanostructured materials over the last two decades. Some of the techniques through which surface microstructure can be modified are ultrasonic shot peening (USSP)/surface mechanical attrition treatment (SMAT), laser shock peening [19, 20], hammer peening [21, 22], surface rolling [23], balldrop [24, 25] roller-burnishing [26] and high speed drilling [27]. Such treatments introduce compressive residual stress and also refine the micro-structure in surface region of the components. In comparison of the usual process of shot peening for inducing residual compressive stress in surface region of the component the process of ultrasonic shot peening induces compressive residual stress to larger depth and also refines the microstructure of the surface region even up to nano scale.

1.6 Ultrasonic Shot Peening (USSP)

Ultrasonic Shot Peening is based on impingement of spherical steel balls on surface of the component, using ultrasonic waves. The balls are placed in a reflecting chamber that is vibrated by a vibration generator. Typical ball sizes are 1-3 mm in diameter, however, they could also be of larger size. The vibration frequency of the chamber is 20 kHz. When the balls are resonated, the surface of the sample to be treated is impacted by a large number

of flying balls over a short period of time. The impact directions of the balls on to the sample surface are random. Each impact (with a velocity of ∼1-20 m/s) induces plastic deformation with a high strain rate in surface region of the sample, as shown schematically in Fig. 1.10. As a consequence, the repeated multidirectional impacts at high strain rates onto the sample surface result in severe plastic deformation and grain refinement progressively down to the nanometer regime in entire surface of the sample [28].

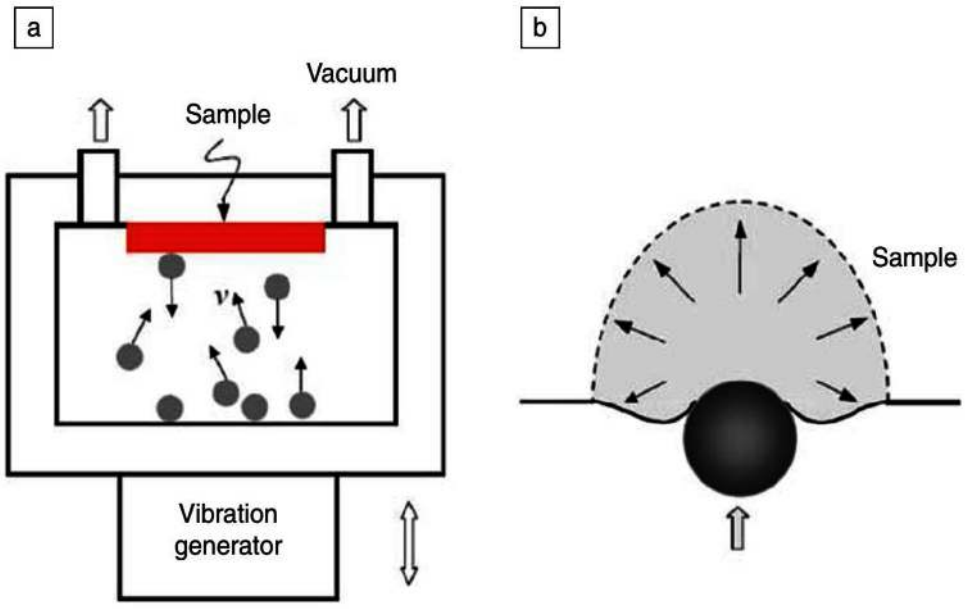

FIGURE 1.10: (a) Schematic of USSP chamber and (b) repeated impact creating surface layer with high strain [28].

Major differences between USSP and conventional shot peening include (1) much larger energy inputs to material surface, (by several orders of magnitude) in USSP, and (2) much larger balls with smooth surfaces that are used in USSP to minimize wearing and damaging the formed nanostructured surface layers. In USSP samples, a gradient in grain-size distribution is generated along the depth from the treated surface, from a few nanometers to micrometers, owing to the gradients in strain and strain rate. In the top most

layer, very high strain rates up to $\sim 10^3 s^{-1}$ can be imposed, inducing extremely fine nano-sized grains distinct from those in the conventional plastic deformation of bulk metals. Finer grains can be induced at higher strain rates, owing to an increased dislocation density and/or nanoscale twinning at high strain rates. USSP is a low-cost process with a unique flexibility to realize a nanostructured surface layer in localized areas on bulk materials or components without shape change. The gradient grain size distribution eliminates the problem of delamination of the nanostructured layers from their matrix.

1.7 Effect of Ultrasonic Shot Peening on Surface Microstructure

It is important to understand the mechanism of surface nanostructuring from ultrasonic shot peening. Due to gradient in strain and strain rate from the treated surface to substrate, a gradual increase occurs in grain size, from a few nanometers to several micrometers without any sharp interface. Several studies have been carried out to characterize the modified microstructure from surface to substrate in different metals and alloys [29–36]. The plastic deformation and dislocation activities in metals and alloys strongly depend on their crystal structures and stacking fault energy (SFE).

Broadly, grain refinement mechanisms of metals are categorized based on their SFE. In metals with high SFEs, dislocation walls and dislocation cells are developed to accumulate strains and consequently sub-boundaries are formed on further straining to subdivide the coarse grains. On the other hand in metals of low SFEs, plastic deformation mode

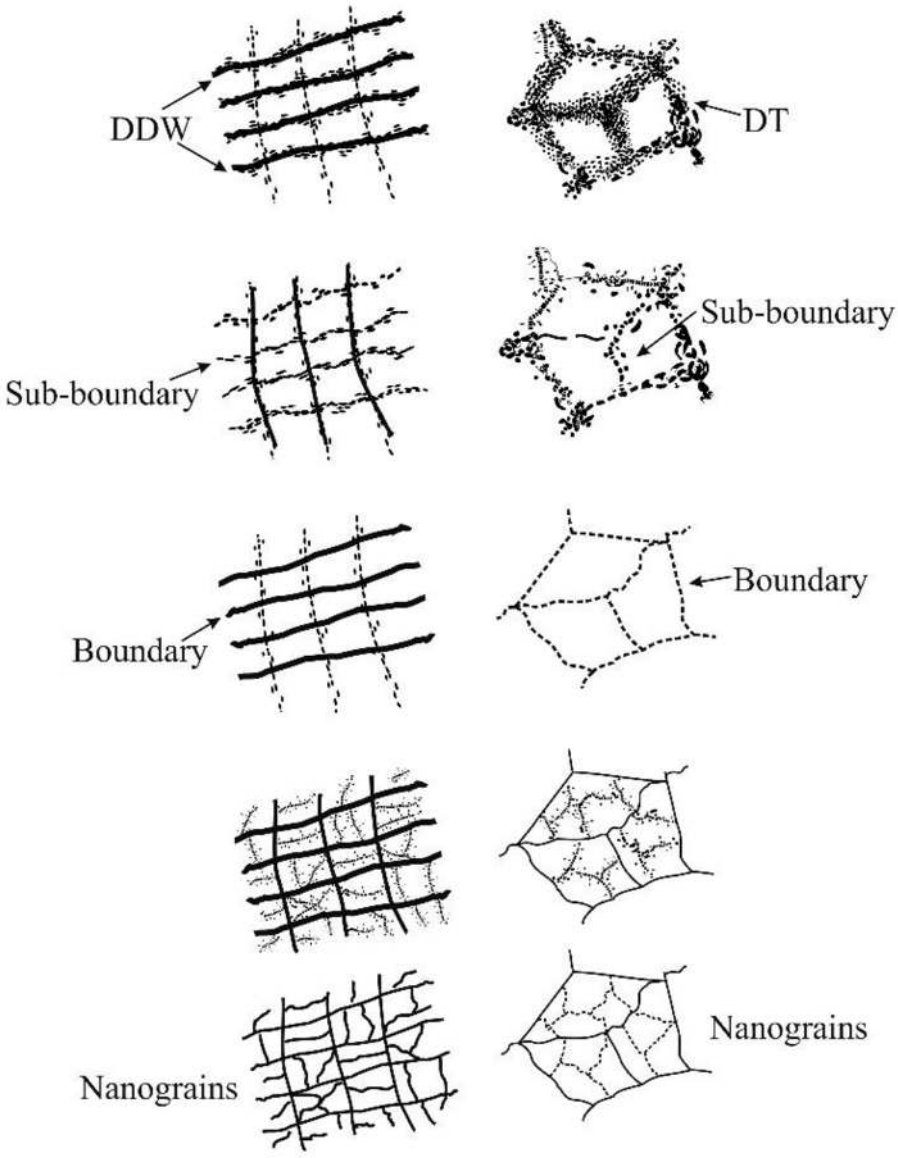

FIGURE 1.11: Schematic illustration of grain refinement via DDW and DT [37].

may shift from dislocation slip to mechanical twins under high strain rate and low temperature. Iron is a metal with high SFE of about 200 mJ/m^2 [28]. As shown in Fig. 1.11, firstly formation of dense dislocation walls (DDWs) and dislocation tangles (DTs) occurs and subsequently these DDWs and DTs transform into sub-boundaries and get divided into smaller grains.

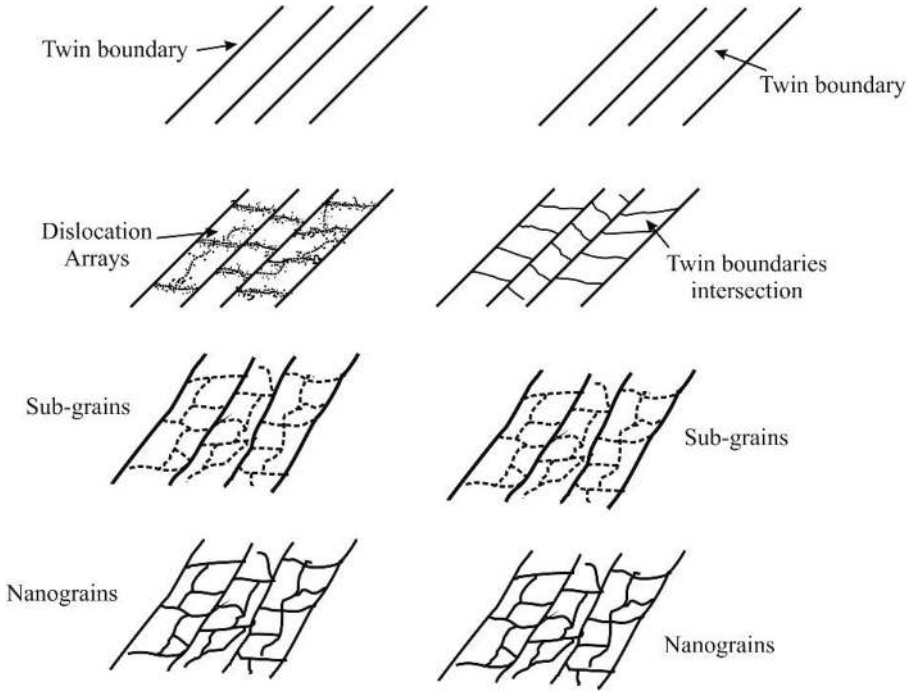

FIGURE 1.12: Schematic illustration of grain refinement by mechanical twins and dislocations resulting from SMAT [37].

Further straining leads to formation of nanostructure with high misorientation.

Copper is a metal with medium SFE of about 78 mJ/m^2 [34]. Initially evolution of dislocation cells (DC) occurs in the deformed region with low strain rates and mechanical twinning results in some grains at favorable orientations. On further straining, DCs transform into sub boundaries with small misorientations and twin boundaries divide the coarse grain into ultrafine structure. AISI 304 stainless steel has very low SFE of 17 mJ/m^2, instead of DDWs as in iron or DCs in copper, there is formation of planar array of dislocations and twins on $\{111\}$ slip plane of austenite phase [38]. Increase in strain results in interaction of twins which leads to further division of the austenite grains into refined blocks (Fig. 1.12). Formation of martensite phase is observed at interactions of twins.

For HCP and FCC metals [32, 33] with low stacking fault energy, high density parallel twins are formed to divide the coarse grain into lamellar twin/matrix alternate blocks. On increasing strain twin-twin interactions lead to division of the grain into rhombic blocks and result into nanometer sized crystallites with large angle boundaries.

The ultrafine-grained microstructures in the surface layer of aluminium alloy 7075 subjected to USSP treatment was studied by Wu et. al [39]. The grain size refines remarkably into the nanometer regime ($<$100 nm) within the outer surface of $\sim$ 22 μm thick. The submicro-grained (0.1–1μm) structure is present in the sub-surface of the layer of $\sim$ 35 μm thick. Next to the strain-free matrix is the extended microbands characterized by elongated subgrains ($>$1μm).

TEM micrograph in Fig. 1.13(a) illustrates the equiaxed microstructure of nanometer size taken at the outer surface of the layer ($\sim$ 8 μm deep from the top surface). The average grain size is determined to be $\sim$ 47 nm. Some grain boundaries are visible but many boundaries are poorly defined. TEM micrograph in Fig. 1.13(b) shows the equiaxed, misoriented, and submicro-sized grains at a depth of increased strain ($\sim$ 40 μm deep from the top). Inset is the ring-like SADP, indicating presence of many small grains with random misorientations. Fig. 1.13(c) shows that the parallel lamellar-type microbands (MBs) of elongated subgrains develop with increasing strain ($\sim$ 60 μm depth from the top surface). MBs have various orientations, due to the change of the strain path. The SADP (Fig. 1.13(d)) shows an undeveloped circle with well-defined diffraction spots, indicating that MBs consist of low angle misorientations [39]. During plastic straining, the formation of subgrains through grain subdivision occurs in order to accommodate

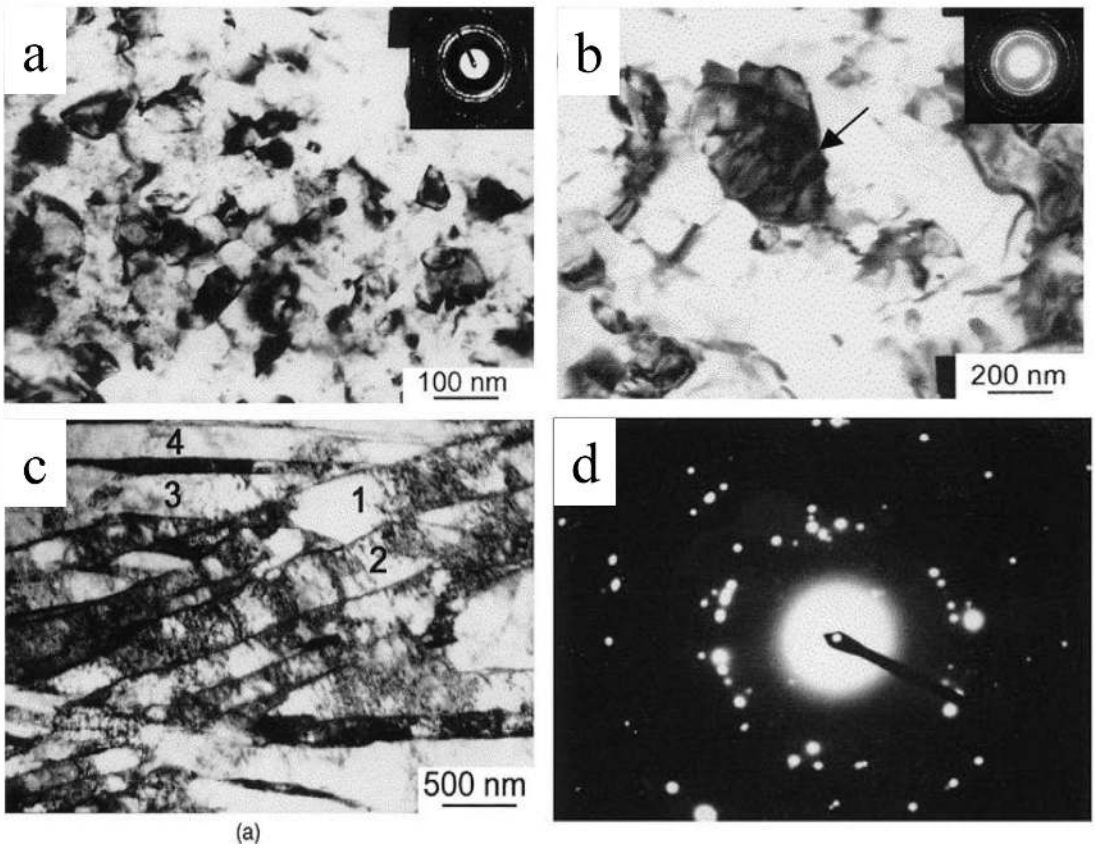

FIGURE 1.13: Microstructure evolution of USSP treated AA7075 at different depths of (a) 8 μm, (b) 40 μm, (c) 60 μm and (d) SADP corresponding to fig. c [39]

the strain. The highly misoriented boundaries are generated by the subgrain rotation for accommodating further deformation.

1.8 Thermal Stability

In recent years, the problem of grain growth in nanocrystalline materials has attracted considerable attention [40–42]. In general, decrease in total energy of the system results in grain growth in polycrystalline materials. The nano sized grains remain in unstable state due to the excess free energy associated with large number of grain boundaries, which is potential driving force for the thermal induced grain growth [43, 44]. The nano

grains spontaneously transform into stable state with increase in temperature, above a critical level and coarsening of grains occurs leading to decrease in the hardness and other mechanical and physical properties. An extremely large driving force is required for the growth of nano-size grains as the driving force for grain growth increases with decrease in grain size [45].

The grain growth mechanism for the nanocrystalline materials is generally related to grain boundary diffusion, as the activation for grain growth is closer to the grain boundary diffusion than that for the lattice diffusion in polycrystalline material [46]. Several investigations have been carried out earlier on thermal stability of nanostructured materials. It was revealed that thermal stability depends both on the type of the material and the processing route. In highly pure metals, the temperature for grain growth is relatively low $\sim$ 0.31-0.38T_m, whereas for the alloy system the grain growth occurs at relatively higher temperature from slow to significant grain growth at 0.50-0.88T_m [45]. Many factors are likely to affect the grain boundary mobility in nanocrystalline alloys, like solute atoms (impurity), second phase (zener) drag, and nanoparticles dragging, and these factors affect the grain growth kinetics. Zhao et al. [47] attributed high thermal stability of the ultrafine grained AA7075 to pinning of the grain boundaries by precipitates. Liu et al. [48] fabricated a nanocrystalline layer in pure Al using SMAT and found that the nanocrystalline surface layer was thermally stable upto 275°C (0.59T_m) and the grain growth took place through grain boundary diffusion. Many nanocrystalline materials are used in industrial applications and the coarsening tendency of these materials inhibit their use in high temperature application, therefore a better understanding of thermal stability

of these nanostructured material is essential.

1.9 Fatigue Behavior of Nanostructured Alloys

Fatigue is one of the largest cause of failure of the structural components and it comprises about 90% of all the metallic failure. Material with fine grain/nanocrystalline surface layer and coarse grain interior is found to possess better resistance to the process of fatigue crack initiation and propagation. A nanocrystalline surface layer can retard the process of fatigue crack initiation whereas, a coarse grain interior lowers the fatigue crack growth rate [49–51]. Moreover, the compressive residual stresses imparted due to ultrasonic shot peening can also retard the process of initiation and propagation of fatigue crack [28, 52]. There have been several literature on the improvement of fatigue life through surface modification of different metals and alloys in high cycle fatigue regime [53–57], however, in the low cycle fatigue regime it is barely explored. The effect of a nanocrystalline surface layer on the fatigue behavior of 316L stainless steel was investigated by Roland et al. [30]. The specimens were treated with spherical shots of 2 mm and 3 mm diameter and the tests were carried out at room temperature under stress control with zero mean stress (R= -1) at a frequency of 10 Hz. Post annealing treatment was given to some specimens after surface mechanical attrition treatment (SMAT). As shown in Fig. 1.14 fatigue strength of the nanostructured stainless steel for all the treated conditions was increased considerably compared to the untreated material. Improvement of about 21% in fatigue limit was achieved for 3 mm diameter balls and further 5-6% improvement was observed with post annealing treatment. For the as-SMATed specimens the improvement

in fatigue life was due to the formation of nanocrystalline surface layer comprising of strain induced martensite and the compressive residual stresses, which enables the surface layer to resist against fatigue initiation and propagation. Subsequent annealing treatment at 400°C relaxes the compressive residual stresses but enhance the ductility and volume fraction of martensite, which ultimately results in furthermore enhancement in fatigue life.

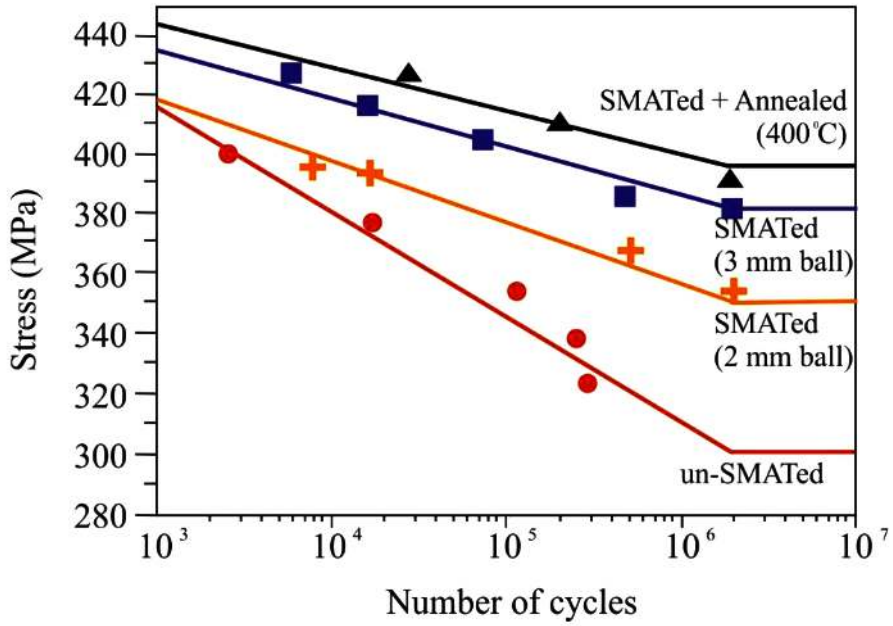

FIGURE 1.14: S/N curves of different SMATed samples and SMATed samples combined with annealing [58].

Shaw et. al [58] studied the effect of two surface modification techniques, surface severe plastic deformation (S^2PD) and shot peening (SP), on the fatigue resistance of nickel base superalloy C-2000. Both the techniques showed better fatigue resistance than the un-treated, and the results showed that S^2PD is more effective in improving the fatigue limit than SP. S^2PD treatment generates thicker nanocrystalline surface layer upto a much

deeper depth and larger compressive stresses than SP which resulted in better fatigue resistance. In an other work, alloy C-2000 was treated for durations of 30, 60, 90 and 180 min and was cyclically loaded. Treatment time of 30 min resulted in the improvement in the fatigue resistance, while prolonged treatments of 60, 90, and 180 min lead to decrement in the fatigue resistance [59]. Therefore, it is also important to optimize the processing parameters of different surface modification techniques as over processing could lead to degradation in fatigue life instead of the improvement [60].

Recently, there have been some work on the effect of surface modification on low cycle fatigue behavior of aluminium alloys. Effect of Ultrasonic Shot Peening (USSP) on LCF behavior of the aluminium alloy 2014 was studied in the peak aged condition [61]. The alloy was subjected to USSP treatment with balls of 3 mm diameter for the duration of 10 minutes and was tested for LCF under total strain controlled mode at room temperature. After USSP, stress relieving treatment was also given to the specimen to see the effect of residual stresses on the fatigue performance. Significant improvement was observed in the LCF life of the USSP treated samples and the percent increment in LCF life increased with decrease in the strain amplitude (Fig. 1.15).

Enhancement in fatigue life was due to the formation of nano crystallites of 30 nm size and also from the large induced compressive residual stresses near the surface region. After stress relieving treatment there was further enhancement in LCF life than that of the USSP treated condition. Tensile residual stresses generated by the USSP treatment were completely relieved after the stress relieving treatment and there were only compressive stresses even at greater depth which retarded the fatigue crack growth rate and enhanced

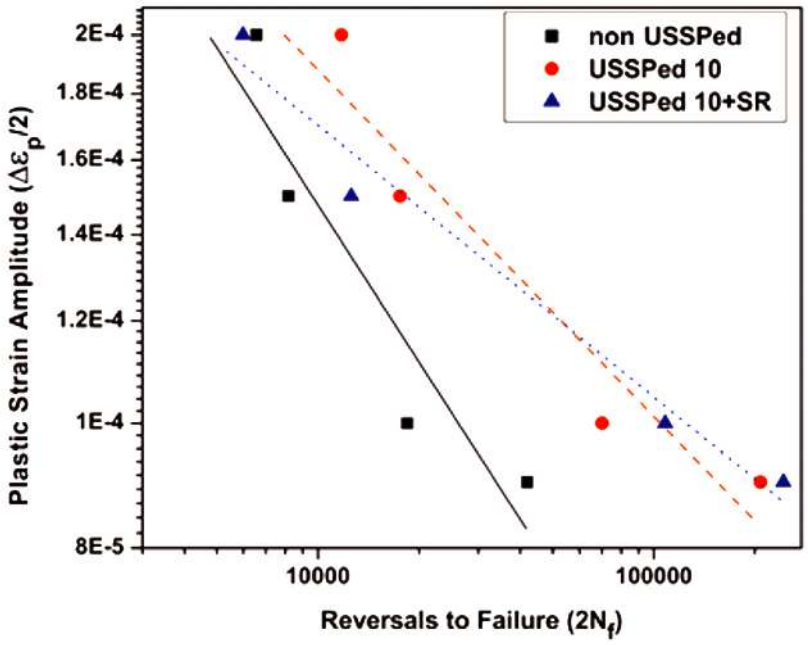

FIGURE 1.15: Variation of fatigue life with plastic strain amplitude [61].

the fatigue life.

Rai et. al [62] examined the effect of USSP on LCF behavior of a high nitrogen austenitic stainless steel under total strain control. The specimen were subjected to USSP for 10 minute. At high strain amplitudes of ±0.73% LCF life of USSP treated specimen was comparable to that of the un-shot peened specimen (Fig. 1.16) but decreased drastically with decrease in strain amplitude due to crack formation on the surface from the post USSP treatment. Cracks were formed due to excessive work hardening near the surface region because of severe impact of the steel balls for 10 minute. Due to this there was an increment in average surface roughness which overcame the beneficial effect of compressive residual stresses and resulted in decrease of LCF life.

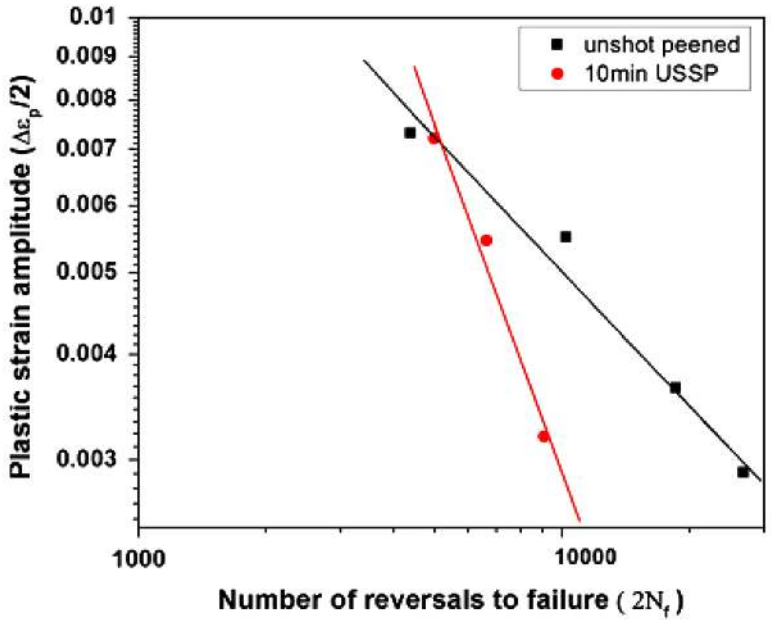

FIGURE 1.16: Coffin-Manson plot of high nitrogen stainless steel for the un-shot peened and 10 min shot peened specimens [62].

1.10 Corrosion Behavior

The aluminium alloy 7075 possesses highest strength among all the wrought aluminium alloys. However, due to the age hardening Al alloys become susceptible to different forms of corrosion such as stress corrosion cracking, pitting corrosion, inter-granular corrosion especially in chloride environment [63–65]. In these alloys corrosion occurs due to presence of intermetallic particles acting either anodic or cathodic with respect to the matrix [66, 67]. Al and its alloys possess good corrosion resistance because of dense and adherent layer of protective aluminium oxide on the surface. Some studies have been carried out on the effect of grain refinement at surface, on corrosion behavior of aluminium alloys, however, no attention has been paid on optimization of the process parameters for high corrosion resistance. It has already been well established by many investigators

that fine-grained structure with more number of grain boundaries promotes passive layer formation and results in enhancement of corrosion resistance [68–70]. However, some adverse effects have also been reported [71, 72].

In the case of aluminium alloys, surface with nanostructure provides better corrosion resistance due to formation of dense passive films as compared with that of coarse grained surface [73]. Wen et.al [74] compared corrosion behavior of the 2024 Al alloy in 3.5 wt%NaCl, SMATed with steel and ceramic balls and observed nano structure in surface region in both the cases. SMAT with steel balls, however, generated less protective Fe containing surface layer causing detrimental effect on corrosion. On the other hand, a dense passive film was formed with the use of ceramic balls and the corrosion resistance was enhanced. The higher corrosion resistance of the ultrafine grained materials may be attributed to decrease in grain size of the alloy with increase in density of diffusion paths for the alloying elements to migrate at the surface and form passive layer [36]. Krawiec et al. [75] reported increase in charge transfer and in resistance of oxide film on AA2058-T8 due to presence of compressive residual stress resulting from laser shock peening treatment. High density of dislocations and grain boundaries provide active sites for easier formation of passive film whereas compressive residual stress makes the passive layer stable and integrated in respect of the untreated coarse grained counterpart. Chen et al. [76] reported that from machine hammer peening of the nickel base alloy 718 there was less surface roughness, larger compressive stress associated with formation of nano grains and nano twins in the surface region to cause improvement in corrosion resistance.

In stainless steels, strain induced martensite transformation resulting from deformation by SMAT/USSP, also had significant role on their corrosion resistance [77, 78]. Thangraj et al. [79] reported increased surface roughness, increase in martensite phase, presence of defects/dislocations, resulting from SMAT with balls of 5 and 8 mm diameter causing lowering of corrosion resistance of the 304 stainless steel. Thus, it is obvious that nanostructure of the surface region is not the only factor to affect corrosion behavior of metallic materials but there are also other factors to affect the same.

1.11 Scope of the Present Investigation

There is very limited literature available on the effect of Ultrasonic shot peening on microstructural modification of AA7075. Also, there is no literature available on the thermal stability of the nanostructured surface layer developed by this surface modification technique. No investigations have been carried out on LCF behavior of the AA7075 in particular at lower strain amplitudes. Little attention has been paid on the effect of USSP on the corrosion behavior and the optimization of the USSP parameters for improving the corrosion resistance. Also, there is no literature on stress corrosion cracking resistance of surface modified AA7075. Therefore, it is needful to carry out systematic investigation on the role of USSP on microstructure, low cycle fatigue and corrosion behavior.

1.12 Objectives of the Present Investigation

The objectives of the present study are the following

- In-depth microstructural characterization of USSP treated samples to determine optimum parameters for achieving nanostructure in AA7075.
- To investigate thermal stability and microstructural evolution of the USSP treated AA7075.
- Investigation of the role of ultrasonic shot peening treatment duration for enhancing low cycle fatigue (LCF) life.
- Study the role of thermal treatments, pre- and post- USSP to reduce the associated residual compressive stress and the modification of microstructure on low cycle fatigue behavior.
- Influence of ultrasonic shot peening on corrosion behavior in 3.5 wt% NaCl solution.
- To optimize USSP duration for enhancement in corrosion resistance.
- Investigation of stress corrosion behavior of USSP treated AA7075 in 3.5 wt% NaCl solution.